Streamwise structure was observed in the initial portion of the mixing layers. However, because of interactions with the walls of the duct, the dominant streamwise structures observed were the collections of vorticity in the corners of the duct. It is not clear from our results what the influence of the corner vortices is on the mixing process. Spanwise vortical rollups, similar to those typically seen in normal mixing layers, have also been observed.[4]

Mixing improved when the stream with greater skew also was the faster stream. An effective-growth-rate parameter λ was applied, and the results suggest that λ is a useful parameter for simultaneously incorporating speed ratio and skew angle into an effective shear.

References

[1]Hackett, J. E., and Cox, D. K., "The Three-Dimensional Mixing Layer Between Two Grazing Perpendicular Streams," *Journal of Fluid Mechanics*, Vol. 43, Aug. 1970, pp. 77–96.

[2]Grundel, H., and Fiedler, H. E., "The Mixing Layer Between Non-Parallel Streams," *4th European Turbulence Conference Abstracts*, Delft Univ. of Technology, Delft, The Netherlands, 1992, pp. 27–29.

[3]Lu, G., and Lele, S. K., "Inviscid Instability of a Skewed Compressible Mixing Layer," *Journal of Fluid Mechanics*, Vol. 249, April 1993, pp. 441–463.

[4]Fric, T. F., "Skewed Shear Layer Mixing Within a Duct," AIAA Paper 95-0869, Jan. 1995.

[5]Van Cruyningen, I., Lozano, A., and Hanson, R. K., "Quantitative Imaging of Concentration by Planar Laser-Induced Fluorescence," *Experiments in Fluids*, Vol. 10, No. 1, 1990, pp. 41–49.

Supersonic Separation with Obstructions

S. B. Verma* and Vijay Gupta†
Indian Institute of Technology, Kanpur 208 016, India

Introduction

THE complex problem of the supersonic flow along a flat plate as it interacts with blunt obstructions has recieved considerable attention.[1,2] The presence of a blunt obstruction in supersonic flow causes the formation of a bow shock wave ahead of the obstruction. The adverse pressure gradient resulting from the bow shock wave propagates upstream in the subsonic flow within the boundary layer and results in the separation of the boundary layer and formation of vortices ahead of the obstruction. These vortices scavenge the boundary layers leading to increased pressures and heat transfer loads.

Various attempts have been made to correlate the separation distance S, which is defined as the distance from the leading edge of the obstacle to the primary separation line, ahead of the obstacle to the height H of the obstacle.[3,4] According to Sedney and Kitchens[5] the most important dimensionless parameters that have significant effect on S/D values are the ratio H/D and Mach number M of the flow. The value of S/D has been observed to increase with M, though the dependence has been found to be weak.[6] A significant effect of H/D on S/D values has been reported. The value of S/D has been observed to increase with increase in H/D values until a point where it approaches an infinite effective height case, after which S/D assumes a constant value, independent of H/D.

Experimental Apparatus and Test Conditions

The experiments were carried out in the 0.18×0.13 m supersonic wind tunnel of the Indian Institute of Technology, Kanpur. This facility is an intermittent, blowdown type wind tunnel. The models used in the present study consisted of obstacles of various sizes (heights H and diameters D) and shapes (circular cylinders and rectangular blocks) mounted on a splitter plate that was carefully aligned with the flow direction (Fig. 1). The leading edge of the plate was made sharp with an angle of 10 deg on the lower side so as to ensure supersonic flow over the plate. The shock wave from the leading edge was seen to be attached and weak enough to be neglected. Thus, the system produced a flow parallel to the plate at the specified Mach number. The plate spanned the width of the tunnel, and the clearance between the plate edges and side walls was sealed using a shaped rubber-gasket mounted flush with the surface. The model protuberances were mounted on the flat plate at two different distances from the leading edge. This enabled experimentation with two different boundary-layer thicknesses.

All of the tests were conducted at a single Mach number value of 1.6 ± 0.1 and at a constant stagnation pressure of 49.0 ± 0.1 psia. The stagnation temperature was fairly constant for all flows, being 13 ± 0.5°C. The unit Reynolds number for the given test conditions was $(3.6 \pm 0.2) \times 10^7$ m^{-1}. Thus, the two test lengths $X_1 = 11 \pm 0.1$ cm and $X_2 = 24 \pm 0.1$ cm gave $Re_{X_1} = (3.97 \pm 0.23) \times 10^6$ and $Re_{X_2} = (8.68 \pm 0.52) \times 10^6$ for the boundary-layer flows. The onset of turbulence usually occurs at length Reynolds number range[7] of 5×10^5–3×10^6. The freestream turbulence in the tunnel used is quite high, of the order of 0.5%. Under such conditions, transition can be assumed[8] to occur at $Re_X = 1.1 \times 10^6$. The length Reynolds numbers obtained in our case, therefore, suggest that the boundary layer can be taken as fully turbulent. The boundary-layer thicknesses are estimated by the procedure suggested by Van Driest[9] for Mach number greater than unity. The corresponding boundary-layer thicknesses, therefore, turned out to be $\delta_{X_1} = 2.0 \pm 0.1$ mm and $\delta_{X_2} = 3.7 \pm 0.1$ mm. The uncertainty in measurement of quantities such as Y, D, and S is ± 0.1 cm.

Results and Discussions

Figure 2 shows the typical flow pattern as developed from the surface flow studies. These surface flow patterns reveal a primary separation line as observed by Ozcan and Holt[10] in the Reynolds number range of 10^6. Immediately behind the primary separation line, the flow in front of the obstacle is radially outward but becomes largely circumferential away from the medial line. One important feature not referred to by any observer is a thick pigment line running parallel to the primary separation line. This can be termed as a neck compression shock, representing the coming together of streamlines because of the limited side flow/pressure relief afforded by the three-dimensional nature of the obstruction. For obstacles of large heights, a reattachment line was observed very close to

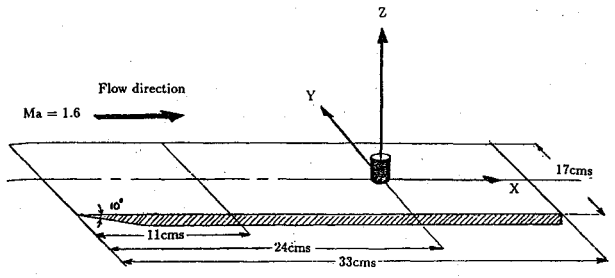

Fig. 1 Isometric view of the plate model.

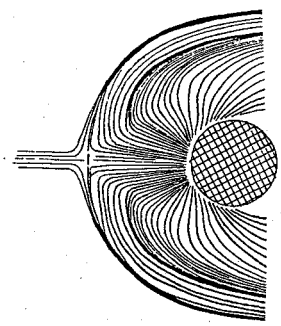

Fig. 2 Typical flow pattern as developed from surface flow studies.

Received Dec. 10, 1994; revision received March 25, 1995; accepted for publication June 12, 1995.

*MTech Student, Department of Aerospace Engineering.
†Professor, Department of Aerospace Engineering.

the leading edge, and the pattern behind this was characterized by burn mark on the pigment representing elevated temperatures in the stagnation flow immediately ahead of the obstacle. The flow pattern thus seen corresponds exactly to the three-layer model proposed by Halprin.[3]

From the data obtained from surface flow patterns, it is observed that the separation distance S has dependence on height H and diameter D of the cylinder and, finally, on the boundary-layer thickness δ.

Various nondimensionalizations have been attempted in the literature. One of the most common is to nondimensionalize all lengths by D, the diameter of the obstruction. This, however, does not give satisfactory results as the effect of X has not been absorbed, and the data for the two X do not converge onto one line. A better nondimensionalization has been attempted by Sedney,[1] who nondimensionalized H and D by δ but S by D.

Such a plot demonstrates that the separation distance S increases for low values of H/δ and then settles down for larger values of H/δ. In fact, most of the increase in S/D occurs for $H/\delta < 1$, i.e., when the obstacle is submerged in the boundary layer. In analyzing the data it appears to us that the height H must be nondimensionalized by δ as was done by previous investigators, but the length scale chosen for nondimensionalizing the separation distance S cannot be D but some measure of the blockage area that is ultimately responsible for producing the separation. Use of $\sqrt{(DH)}$ did not lead to a worthwhile result, but $\sqrt{(D\delta)}$ resulted in Fig. 3, wherein all of the points for various D, H, and, significantly, δ collapse essentially on to one curve. The various points can be correlated by the following relationship:

$$S/\sqrt{(D\delta)} = 0.736(H/\delta) - 0.036(H/\delta)^2$$

Thus, it is clear that the separation distance S depends on the length scale of the blockage presented to the boundary layer and on the height H of the cylinder with respect to the boundary-layer thickness. Generalizing for the entire range of H, we emphasize that the appropriate length scale for separation distance S is $\sqrt{(DH')}$, where H' is H if $H < \delta$ and δ if $H > \delta$. Thus, the diameter of the cylinder has no direct role to play. Accordingly, the standard correlation reported by Westkaemper[4] and used thus far has to be modified. The reason why this effect had so far been missed by others appears to be that no investigator apparantly has taken data at two different boundary-layer thicknesses.

The variations in the maximum lateral extent Y of the separation line, like for S, are dependent on H, D, and δ. Nondimensionalizing the independent variable with respect to δ and dependent variable with respect to D, we obtain Fig. 4. It can be noted that the dependence on D/δ is rather weak, so that we can develop an approximate correlation as

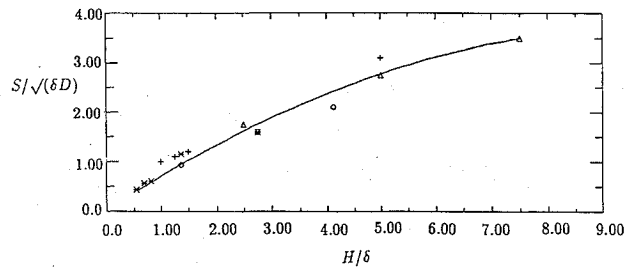

Fig. 3 Variation of $S/\sqrt{(\delta D)}$ with H/δ, where D = 32 mm: X_2, ○ and X_1 △; D = 17 mm: X_2, ∗ and X_1 +.

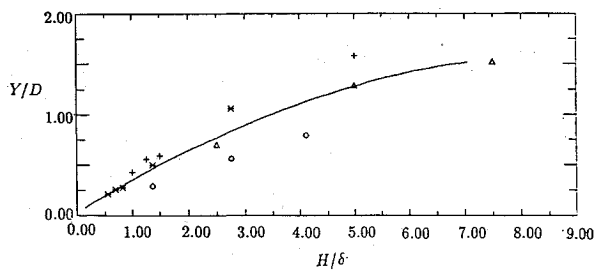

Fig. 4 Variation of Y/D with H/δ, where D = 32 mm: X_2, ○ and X_1 △; D = 17 mm: X_2, ∗ and X_1 +.

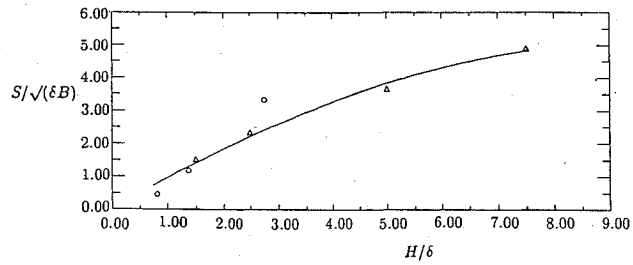

Fig. 5 Variation of $S/\sqrt{(\delta B)}$ with H/δ, where D = 32 mm: X_2, ○ and X_1, △.

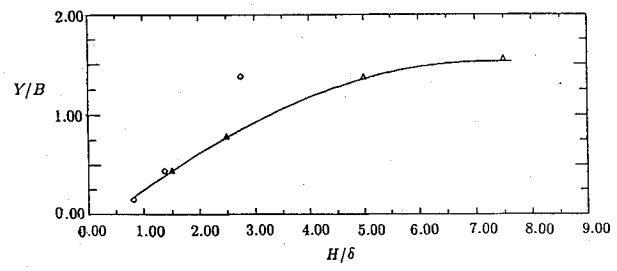

Fig. 6 Variation of Y/B with H/δ, where B = 32 mm: X_2, ○ and X_1, △.

$$Y/D = 0.356(H/\delta) - 0.02(H/\delta)^2$$

We are unable to find any data in the literature for rectangular blocks. Data shows greater separation distance S when compared with a circular cylinder of the same H and D at the same X location. On the basis of similar reasoning as given for circular cylinders, we have developed a correlation for the separation distance S for rectangular blocks as

$$S/\sqrt{(\delta B)} = 1.017(H/\delta) - 0.05(H/\delta)^2$$

where B is the width of the rectangular block presented to the oncoming flow. A plot of this case is shown in Fig. 5.

Similarly, for the maximum lateral extent of the separation line Y for rectangular blocks (Fig. 6), we get a correlation as

$$Y/B = 1.7 - 2.06\exp[-0.342(H/\delta)]$$

Conclusions

Correlating the data obtained from surface flow patterns we conclude that the appropriate length scale for H is δ and that for S is a length based on the boundary-layer blockage area δD. Thus, when $S/\sqrt{(\delta D)}$ is plotted against H/δ, all points collapse quite well on to a single curve for the various values of D, H, and δ. We thus emphasize that the appropriate length scale for separation distance S is $\sqrt{(DH')}$, where H' is H if $H < \delta$ and δ if $H > \delta$. Thus, the diameter D of the obstruction has no direct role to play and, hence, the standard correlation reported by Westkaemper[4] needs to be modified. Similar explanations hold for the case of rectangular blocks.

References

[1]Sedney, R., "Survey of the Effects of Small Protuberances on Boundary Layer Flows," *AIAA Journal*, Vol. 11, No. 6, 1973, pp. 782–792.

[2]Korkegi, R. H., "Survey of Viscous Interactions Associated with High Mach Number Flight," *AIAA Journal*, Vol. 9, No. 5, 1971, pp. 771–784.

[3]Halprin, R. W., "Step Induced Boundary Layer Separation Phenomena," *AIAA Journal*, Vol. 3, 1965, pp. 357–359.

[4]Westkaemper, J. C., "Turbulent Boundary Layer Separation Ahead of Cylinders," *AIAA Journal*, Vol. 6, No. 7, 1968, pp. 1352–1355.

[5]Sedney, R., and Kitchens, C. W., "Separation Ahead of Protuberances in Supersonic Turbulent Boundary Layers," *AIAA Journal*, Vol. 15, No. 4, 1977, pp. 546–552.

[6]Westkaemper, J. C., "Step Induced Boundary Layer Separation Phenomena," *AIAA Journal*, Vol. 4, No. 6, 1966, pp. 1147, 1148.

[7]Houghton, E. L., and Brock, N. B., *Aerodynamics for Engineering Students*, 1982.

[8]Lin, C. C., *Turbulent Flows and Heat Transfer*, 1959.
[9]Van Driest, E. R., "Turbulent Boundary Layer in Compressible Flows," *Journal of Aeronautical Sciences*, Vol. 18, No. 3, 1951, p. 145.
[10]Ozcan, O., and Holt, M., "Supersonic Separated Flow Past a Cylindrical Obstacle on a Flat Plate," *AIAA Journal*, Vol. 22, No. 5, 1984, pp. 611–617.

Solution-Adaptive Approach for Unsteady Flow Calculations on Quadrilateral-Triangular Meshes

C. J. Hwang* and J. M. Fang†
National Cheng Kung University, Tainan, Taiwan, Republic of China

Introduction

In recent years, considerable effort has been made in the development of solution-adaptive methods for solving the unsteady Euler equations on unstructured meshes. Several impressive approaches,[1–3] which include the numerical schemes and adaptive mesh techniques, were presented to efficiently obtain higher spatial accuracy in the flow solutions on the triangular meshes. Because the use of quadrilateral-triangular meshes is better than that of purely triangular meshes in the study of steady flows,[4] it is worthwhile to create a solution-adaptive approach for unsteady flow calculations on quadrilateral-triangular meshes.

In computation of unsteady flows, adaptive mesh techniques are generally divided into three categories: 1) mesh regeneration,[2] 2) mesh movement,[5] and 3) mesh enrichment.[1,3] Considering accuracy, efficiency, simplicity, and flexibility, the mesh enrichment method is adopted in this work. During the process of mesh enrichment, the following two problems should be addressed: 1) how the flow properties at the nodes and centers of new cells are calculated to obtain the spatially accurate values and 2) when the mesh is refined to achieve the time-accurate solutions. For the first problem, several weighted-averaging procedures[1] and scattered data interpolation approaches[6] were introduced. In the present paper, a minimum norm network (MNN) method, that was formulated on triangular meshes by Nielson and Franke,[6] is modified and applied to interpolate the new node and cell-centered values on quadrilateral-triangular meshes. For the second problem, in most previous works, such as Refs. 1 and 3, the mesh has been spatially adapted every constant time step during the calculations. If this kind of approach is used, the mesh system can not adjust itself simultaneously with the time-varying flow solutions. In other words, the mesh will lag the solution in time. To solve this problem, Bockelie and Eiseman[5] presented a prediction-correction method for grid movement. The data transfer from the old grid to the new grid, however, introduced the numerical error due to the interpolation. Also, extra computer time was required to operate this prediction-correction method. Instead of using the foregoing two approaches, a simple method is presented in this paper. By using this method, the mesh can be properly adapted in time according to the unsteady flow solutions, and the numerical error due to interpolation and extra computer time[5] will be reduced or avoided.

The purpose of this work is to develop a solution-adaptive approach for unsteady inviscid flow calculations on quadrilateral-triangular meshes. This approach includes a locally implicit total variation diminishing (TVD) scheme[4] and an adaptive mesh technique. To evaluate the present interpolation algorithm, sinusoidal, exponential, $(x+y)^2$ and $(x+y)$ functions are tested. Based on the numerical results for the shock propagation in a channel, the present solution-adaptive approach is accurate, reliable, and suitable for studying unsteady inviscid flows.

Received Sept. 24, 1994; revision received June 8, 1995; accepted for publication June 8, 1995; presented as Paper 95-1723 at the AIAA 12th Computational Fluid Dynamics Conference, San Diego, CA, June 19–22, 1995.

*Professor, Institute of Aeronautics and Astronautics, 1 University Road. Member AIAA.
†Graduate Student, Institute of Aeronautics and Astronautics, 1 University Road.

Euler Solution Procedure and Adaptive Mesh Technique

In this work, the two-dimensional unsteady Euler equations are solved in the X–Y Cartesian coordinate system. The locally implicit cell-centered finite volume TVD scheme that was formulated on the quadrilateral-triangular meshes by Hwang and Yang[4] was employed. About the shock propagation in a channel, adiabatic and no-penetration conditions are imposed on the wall surface. The pressure values at the wall are extrapolated from those at the interior cells. The upstream flow condition is imposed, and the flow properties at the exit plane are extrapolated from those at the interior cells.

The present adaptive mesh technique includes an enrichment indicator $|\nabla\rho|$ (magnitude of density gradient), an unstructured mesh generation method,[2] a mesh enrichment method, and an interpolation algorithm. For the mesh enrichment method, a coarse mesh is used as a background grid, and a two-level refinement procedure is created. If the value of $|\nabla\rho|$ for any one of the unrefined cells on the current mesh during the unsteady calculations is larger than a threshold value, the mesh enrichment is operated on the background grid. After finishing the generation of an intermediate mesh, the properties at all added new nodes are interpolated from those at the background nodes. Similar to first-level mesh refinement, second-level refinement on the intermediate mesh is continued. After that, the new computational mesh is completed. The diagrams for possible mesh enrichment situations and the detailed description of the mesh enrichment procedure are given in Ref. 7. Because Webster et al.[3] showed that the mesh coarsening accounted for the majority of the central processing unit (CPU) cost for each enrichment step, the mesh coarsening procedure is not used in this work. According to the preceding discussion, the CPU time due to mesh coarsening and the numerical error arising from the interpolation of flow properties at new nodes are avoided or reduced. Also, the mesh system can adjust itself with time-varying flow solutions. As for the interpolation algorithm, a minimum norm network method that was formulated on triangular meshes by Nielson and Franke[6] is modified and applied to interpolate the new node and cell-centered values during the mesh enrichment on quadrilateral-triangular meshes. With respect to the slopes of flow properties at the nodes, the minmod functions are introduced to eliminate the numerical noise around the shock regions. The mathematical formula and detailed explanations are provided in Ref. 7.

Results and Discussion

To understand the characteristics of present interpolation algorithm, two kinds of triangular-quadrilateral meshes (see Fig. 1) are used to achieve the numerical interpolations for $\sin(x+y)$, $\exp(x+y)$, $(x+y)^2$, and $(x+y)$ functions. For each cell on those two meshes, the coordinates of the centroid and the exact values at related nodes are calculated first. Then the values of $\sin(x+y)$, $\exp(x+y)$, $(x+y)^2$, and $(x+y)$ at those centroids are obtained by using corresponding node values and the present interpolation algorithm. If the test function is linear, such as $(x+y)$, the interpolation errors for the Laplacian weighted-averaging method and present algorithm (see Table 1) are near the machine error (single precision). The accuracy of the Laplacian weighted-averaging method is better than the present algorithm. If the test functions are nonlinear, however, such as $\sin(x+y)$, $\exp(x+y)$, and $(x+y)^2$, the error analysis (see Table 1) indicates that the present algorithm is the best one among three methods. In the computations of unsteady inviscid flows, the Euler solutions are almost nonlinear. Therefore, the present interpolation algorithm is recommended.

To study the accuracy and efficiency of the present solution-adaptive approach on quadrilateral-triangular meshes, shock prop-